(Preprint) AAS 25-588

ISS CONTROL-STRUCTURE INTERACTION MITIGATION STUDY

Amanda N. Macha,*† Kyle J. DeMars,‡ and Jiann-Woei Jang§

The Control Structure Interaction of flexible spacecraft feedback control systems is demonstrated in this paper. A trade study of CSI mitigation strategies is conducted to evaluate their attitude and load performance. An International Space Station configuration is chosen as a testbed for the corresponding performance evaluation. A platform is developed to facilitate CSI strategy evaluation. The platform consists of spacecraft dynamics models, flex filters, and feedback controllers. For the purpose of this paper, the platform models an International Space Station configuration in a 400km circular orbit subject to gravity gradient disturbance torque only. A PID controller, flex filter, and phase plane controller are designed and implemented in the platform. The performance evaluation of these CSI mitigation results are summarized in this paper.

INTRODUCTION

With various vehicles in development that will deliver astronauts to Earth- or lunar-orbiting spacecraft, there is a growing need for augmented control capability using visiting vehicle thrusters. Having a configurable control system capable of handling control-structure interaction (CSI) effects can provide greater flexibility in the visiting vehicle configurations for any spacecraft. The main goal of the augmented control design is to mitigate CSI for mated configuration.

Many CSI alleviation strategies have been studied in the literature (see References 1, 2, and 3) and then demonstrated in International Space Station (ISS) attitude control design.[4] Conventional proportional-integral-derivative (PID) control is known to be feasible for a structure modeling both rigid-body and flex dynamics, as shown in initial control solution considerations for the never-implemented ISS solar dynamic power module. This solution, however, was shown to be sensitive to elastic mode order reduction of the spacecraft plant model, being most feasible for a reduced-order model.[1] A conventional PID controller is suggested to be inadequate for a spacecraft with many elastic modes such as the full ISS. Phase plane control is another common control solution that has been utilized in the ISS for years. Defined by firing regions where control authority is exerted and dead zones where no thruster firings take place, the phase plane controller is a nonlinear controller that offers a method for reducing and optimizing propellant usage while guaranteeing stability.[2,8] Filtering is another key control system component that is often implemented to ensure stability of the control system. Rate filters are commonly designed to maximize bandwidth to optimize system performance while attenuating vehicle flex dynamics and noise.[2,7] These filters are

* Graduate Student, Department of Aerospace Engineering, Texas A&M University, College Station, TX 77843.
† Draper Scholar, The Charles Stark Draper Laboratory, Inc., Houston, TX 77058.
‡ Associate Professor, Department of Aerospace Engineering, Texas A&M University, College Station, TX 77843.
§ Distinguished Member Technical Staff, The Charles Stark Draper Laboratory, Inc., Houston, TX 77058.

not specific to one type of control solution, and can be implemented with many different controller types.

This paper presents the design of a Control-Structure Interaction Mitigation Study Platform (CSIMSP), a generic platform for evaluating the performance of each CSI mitigation solution presented herein. The CSIMSP models both the rigid-body and flex dynamics of a flexible spacecraft. For the purposes of this paper, the platform models the ISS. This paper investigates the performance of three common CSI mitigation solutions: a flex filter; a PID controller; and a phase plane controller. Each controller type is simulated on the developed CSIMSP and evaluated, with the results aggregated into a trade study.

MODEL DESIGN

Rigid Body Motion

The rotational motion of a rigid body is modeled by

$$\dot{\boldsymbol{\omega}} = \boldsymbol{J}^{-1}[\boldsymbol{m} - (\boldsymbol{\omega} \times \boldsymbol{J}\boldsymbol{\omega})] \tag{1}$$

where $\boldsymbol{\omega}$ denotes the angular velocity of the body with respect to the inertial frame, $\boldsymbol{m}$ the applied torques on the body, and $\boldsymbol{J}$ the body's inertia tensor expressed in the body frame.[5] The angular velocity vector $\boldsymbol{\omega}$ has the form $\boldsymbol{\omega} = [p \quad q \quad r]^T$.

Quaternions are utilized as the attitude representation scheme. The quaternion kinematics implemented in the model are

$$\dot{\overline{\boldsymbol{q}}} = \frac{1}{2}\boldsymbol{\omega} \otimes \overline{\boldsymbol{q}} \tag{2}$$

where $\overline{\boldsymbol{q}}$ is the normalized quaternion of rotation describing the current attitude of the body.

Flex Dynamics

The CSIMSP is designed to model spacecraft flex dynamics as well as the rigid body dynamics. Pre-generated flex characteristics of the ISS are utilized in tandem with the rigid body dynamics calculated by the CSIMSP to approximately model the motion of a flexible body. The flex dynamics of the ISS are modeled as a linear time-invariant (LTI) system. The torque applied along each body axis is the system input, and the resulting roll, pitch, and yaw rates from flex motion of the ISS are output. The flex angular rates are then superpositioned with the rigid body angular rates to join the two models together.

Structural Characteristics. A singular value decomposition is performed on the flex model in two groups: 1) the Rotational Jet Command (RJC) to rate gyroscope outputs, and 2) the RJC to normalized structural load limits. Figure 1 shows consistently negative magnitude values for the RJC to rate gyroscope output.

Figure 2 shows the singular value decomposition for the RJC to structural load limit outputs of the flex model. Since the load limits are normalized, any values exceeding 0dB indicate loads that are likely to exceed their limits if not attenuated.

Singular value plots for RJC to specific load groups within the flex dynamics model are also generated. Like the structural load limits, the load group loads are also normalized. Of the 19 load groups created, 5 display singular values greater than 0dB. Figure 3 shows the singular value plot of Group 12, which displays the largest non-negative singular value.

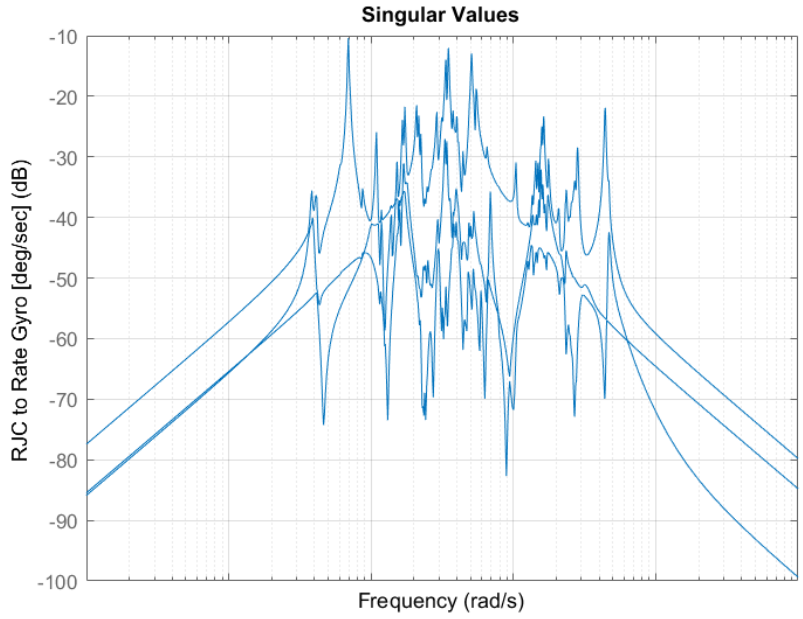

Figure 1. Rotational Jet Command to Rate Gyroscope Output

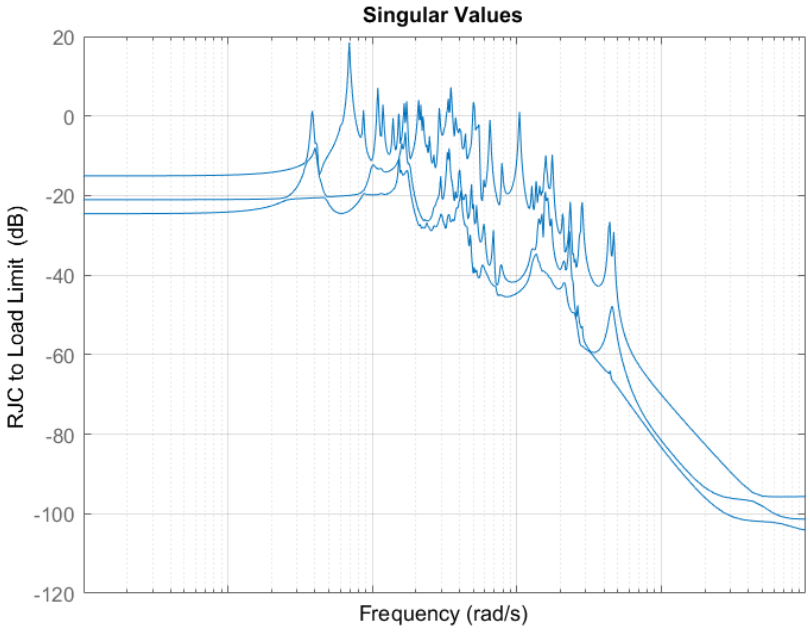

Figure 2. Rotational Jet Command to Normalized Load Limit

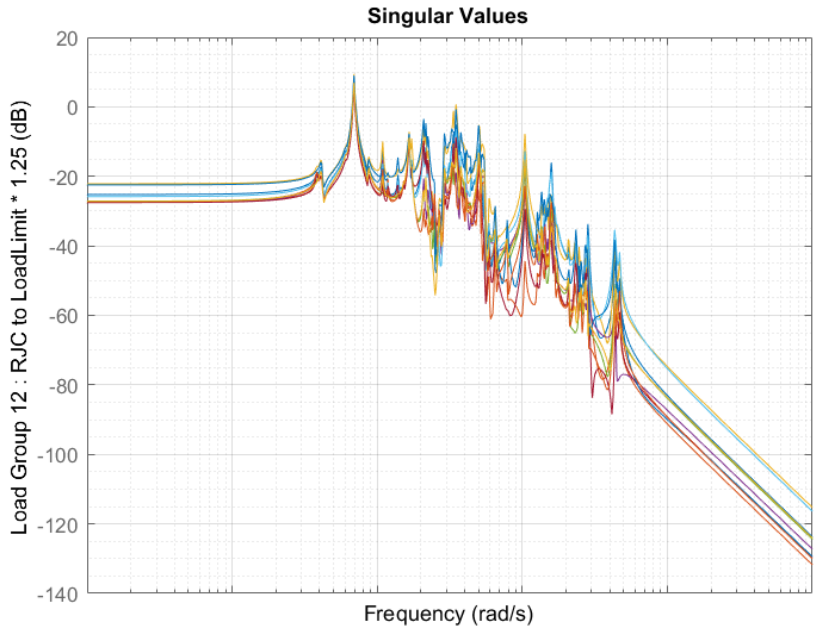

Figure 3. Rotational Jet Command to Load Group 12 Normalized Load Limit

Environmental Torque

Gravity Gradient Torque. The only environmental torque implemented in the CSIMSP is gravity gradient torque, which is given by

$$\boldsymbol{m_{gg}} = 3{\omega_0}^2[\boldsymbol{n} \times \boldsymbol{Jn}], \tag{3}$$

where $\boldsymbol{n}$ is the body frame representation of a nadir-pointing unit vector and ω_0 is the magnitude of the orbital angular velocity.[5] The resulting $\boldsymbol{m_{gg}}$ is substituted into Equation 1 to model rigid-body dynamics with gravity gradient torque.

CSI MITIGATION STRATEGIES

For this work, three CSI mitigation strategies are tested on the CSIMSP: 1) a PID controller, 2) a flex filter, and 3) a phase plane controller.

PID Control

A PID controller is designed for rigid body dynamics only, subject to gravity gradient torque.

The PID controller is implemented using the attitude error signal, the integral of the attitude error signal, and rate error signal as the proportional, integral, and derivative error signals, respectively. The error quaternion is used to calculate the attitude error signal. The error quaternion is given by

$$\overline{\boldsymbol{q}}_{err} = \overline{\boldsymbol{q}}^{-1}_{LVLH \to body,m} \otimes \overline{\boldsymbol{q}}_{LVLH \to body,d} \tag{4}$$

The quaternion describing the measured orientation of the body frame with respect to the LVLH frame, $\overline{\boldsymbol{q}}_{LVLH\rightarrow body,m}$, is a known output from the rigid body equations of motion. The quaternion describing the desired orientation of the body frame with respect to the LVLH frame, $\overline{\boldsymbol{q}}_{LVLH\rightarrow body,d}$, is defined as the attitude the CSIMSP is commanded to hold. Given the error quaternion $\overline{\boldsymbol{q}}_{err}$, the small quaternion approximation is utilized to calculate the rotation angle error. The small quaternion approximation is given as

$$\overline{\boldsymbol{q}} \approx \widehat{\overline{\boldsymbol{q}}} = \begin{pmatrix} 1 \\ \mathbf{0}_3 \end{pmatrix} + \frac{1}{2}\begin{pmatrix} 0 \\ \delta\boldsymbol{\theta} \end{pmatrix}$$

For sufficiently small quaternions, the rotation angle error is extracted from the quaternion approximation's vector part[6] and can be expressed as

$$\delta\boldsymbol{\theta} = 2 * \{\widehat{\overline{\boldsymbol{q}}}\}$$

where $\{\widehat{\overline{\boldsymbol{q}}}\}$ is the vector part of the quaternion $\widehat{\overline{\boldsymbol{q}}}$. This angle error is fed into the PID controller as the proportional error signal. The derivative error signal is the angular velocity of the LVLH frame with respect to ECI.

PID Gains. The PID gains are selected to be

$$K_p = -(n\omega_0)^2$$

$$K_i = 0.001 * K_p$$

$$K_d = -2\zeta n\omega_0$$

where n is a design variable, $\zeta = 0.7$, and ω_0 is the magnitude of the initial orbit angular velocity.[4]

To accurately model real spacecraft thruster capabilities, a deadzone is implemented into the PID controller inputs and outputs. Angle errors smaller than 1 deg and rate errors smaller than 0.1 deg/s are considered to be zero error. In addition, torque outputs smaller than 20% of the maximum output torque are considered to be zero. This ensures that no controller action is taken within the deadband and that realistic thruster capabilities are modeled.

Flex Filter

High-frequency flex dynamics have the potential of making the system unstable. Because of this, a low-pass filter and notch filter are implemented to attenuate the high-frequency flex modes while maintaining attitude control.[2]

The implemented flex filter is a rate filter. The rates along each axis are passed through both low-pass filters and notch filters designed in continuous-time and then discretized.

Phase Plane Control

Pulse-width modulation (PWM) and firing delay logic have long been implemented by ISS attitude hold controllers in conjunction with phase-plane control methods.[4] Control for these on-off types of systems, called reaction control systems (RCS), generally involves a deadzone to avoid high-frequency thruster firing patterns that excite spacecraft flex frequencies. This deadzone is implemented in the form of a phase plane. With a known error quaternion $\overline{\boldsymbol{q}}_{err}$ and known rotational rate error vector $\boldsymbol{\omega}_{err}$, attitude error per axis is plotted against rate error per axis. This creates a deadzone around the commanded attitude state (the origin). An allowed attitude error called the deadband and allowed rate error called the Rate Limit (RL) are determined. No control action is taken for errors within these bounds.[7,8]

Attitude error is calculated with the same method utilized by the PID controller in calculating the error quaternion. The acceptable attitude error threshold, or 'deadband', is chosen such that any high-frequency flex modes of the plant will not become excited by RCS thruster firings. For the CSIMSP, the attitude deadband δ is set at 1 deg.

The rate limits are also calculated using the same method utilized in the PID controller to calculate $\boldsymbol{\omega}_{err}$. Like the attitude error limits, the acceptable RL threshold is chosen such that any high-frequency flex modes of the plant will not become excited by RCS thruster firings. The phase plane controller is designed with a drift channel rate limit of 0.1 deg/s.

The phase plane deadzone is defined by switching lines that denote when thruster firings should occur as well as the direction of the firings. These switching lines are equal to the positive and the negative of the attitude deadband δ. The deadband rate limits, $\boldsymbol{\omega}_{db}$, are given by

$$\boldsymbol{\omega}_{db} = \sqrt{2\delta\boldsymbol{\alpha}} \tag{5}$$

where α is given as

$$\boldsymbol{\alpha} = \boldsymbol{J}^{-1}\boldsymbol{T}$$

and $\boldsymbol{T}$ is an array of the allowable control torque magnitude about each axis.

Thruster firings occur whenever either of the inequalities given as

$$k_p\theta + k_d\dot{\theta} < -\delta \tag{6}$$

$$k_p\theta + k_d\dot{\theta} > \delta \tag{7}$$

are true. In both cases, $k_p = 1$, $k_d = \frac{\delta}{\boldsymbol{\omega}_{db}}$, θ is any arbitrary angle error, and $\dot{\theta}$ is any arbitrary angle rate error. When the inequality in Equation 6 is true, a positive firing is commanded, and a negative firing is commanded when the inequality in Equation 7 is true. Equation 6 and Equation 7 are analogous to PD controllers, with k_p as the proportional gain and k_d as the derivative gain.

SIMULATION RESULTS

Using the developed platform and controllers, the following results are generated. All results are generated on the CSIMSP modeling the ISS in a 400km circular orbit.

Uncontrolled Motion

This section details the simulation results of an uncontrolled rigid-body model and uncontrolled flex body model of the ISS. For the purposes of this section, the starting attitude with respect to the LVLH frame in $[roll, pitch, yaw]$ Euler angles is $[\phi, \theta, \psi] = [0 \quad 0 \quad 0]$ deg and starting angular velocity is $\boldsymbol{\omega} = [0 \quad 0.063 \quad 0]$ deg/s.

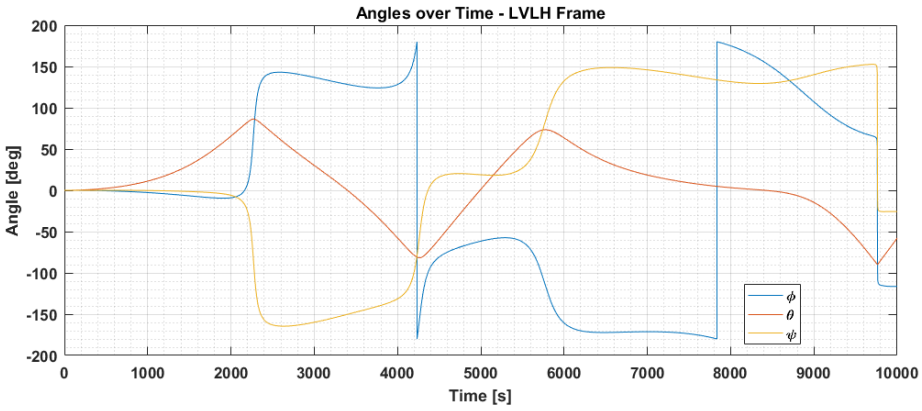

Figure 4. Body Frame Orientation with Respect to LVLH Frame for Uncontrolled Rigid-Body Motion.

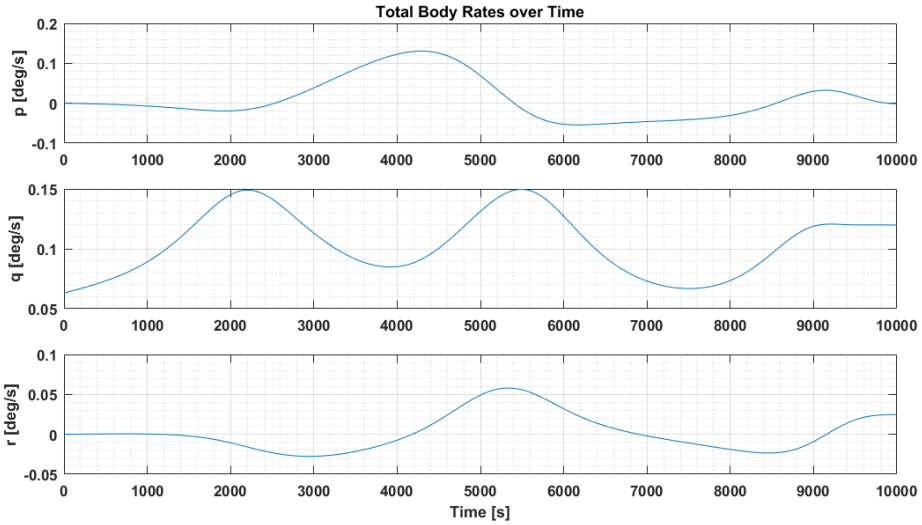

Figure 5. Body Rate with Respect to LVLH Frame for Uncontrolled Rigid-Body Motion

Rigid Body Motion. Rigid-body dynamics with gravity gradient torque is simulated for the ISS in a 400km altitude circular orbit. The time history of the body frame attitude with respect to the local-vertical local-horizontal (LVLH) frame is shown in Figure 4. It should be noted that because the attitude is propagated using quaternions, all rotation angles are bounded between ±180 deg. The time history of the components of the angular velocity vector is shown in Figure 5.

Without a controller, the ISS attitude and angular velocity diverge from their initial states.

Rigid Only Cases

PID Controller

The developed PID controller is implemented on the CSIMSP with only rigid body dynamics and gravity gradient torque. The controller functions as an attitude hold controller, tracking a

constant desired attitude expressed in the LVLH frame. For the purposes of this section, the desired attitude with respect to the LVLH frame is $[\phi, \theta, \psi] = [0 \quad 0 \quad 0]$ deg, which is an alignment of the ISS body frame to the LVLH frame.

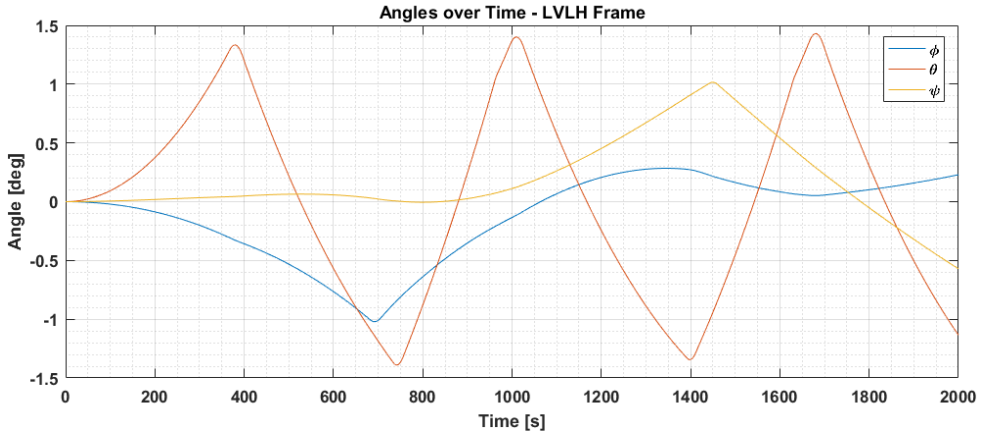

Figure 6. Body Frame Orientation with Respect to LVLH Frame with PID Control for Rigid-Body Motion

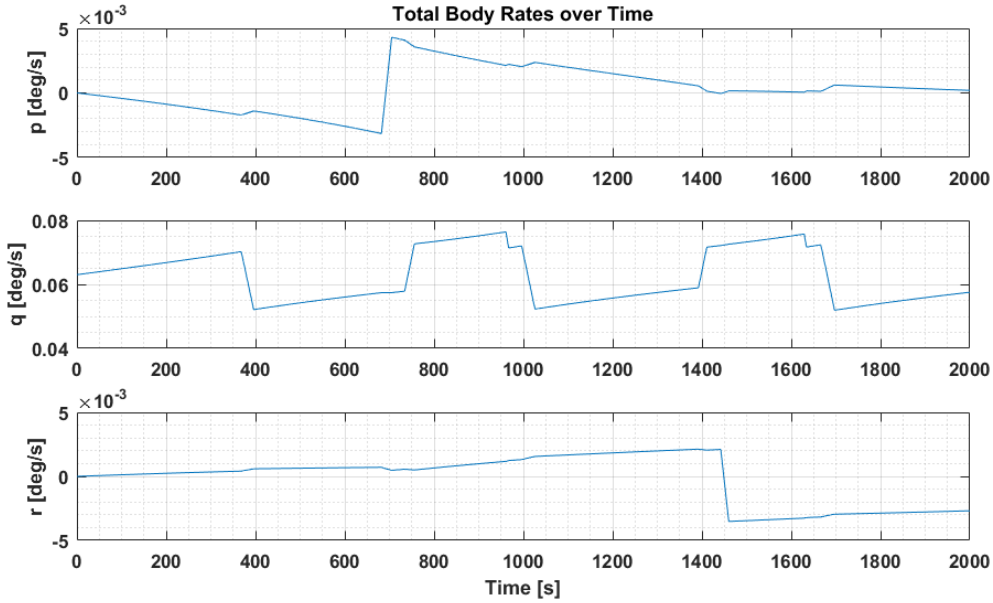

Figure 7. Body Rate with Respect to LVLH Frame with PID Control for Rigid-Body Motion

Figure 6 shows the results of the PID attitude hold controller on the attitude of the ISS body frame with respect to the LVLH frame. The designed PID controller successfully holds the space-craft attitude along all axes to within at least 1.5 degrees of the desired attitude. The spacecraft is also not subject to any large rates, as shown in Figure 7.

Phase Plane Controller.

A three-axis phase plane controller is designed and implemented on the CSIMSP. The phase plane controller is designed with a drift channel rate limit of 0.1 deg/s and attitude deadband δ of 1 deg/s. Like the PID controller, the phase plane controller functions as an attitude hold controller, tracking a constant desired attitude expressed in the LVLH frame. For the purposes of this section, the desired attitude with respect to the LVLH frame is $[\phi, \theta, \psi] = [0 \quad 0 \quad 0]$ deg. The controller is implemented on the CSIMSP with rigid-body dynamics only with gravity gradient torque.

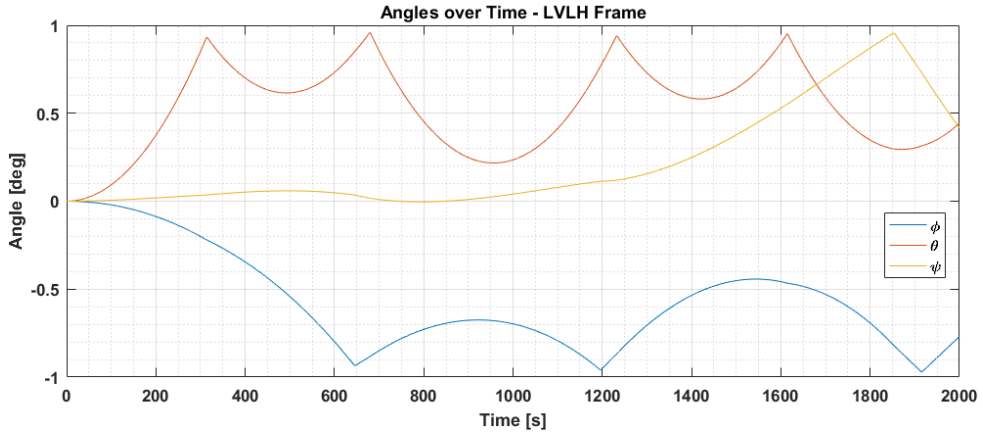

Figure 8. Body Frame Orientation with Respect to LVLH Frame with Phase Plane Control for Rigid-Body Motion

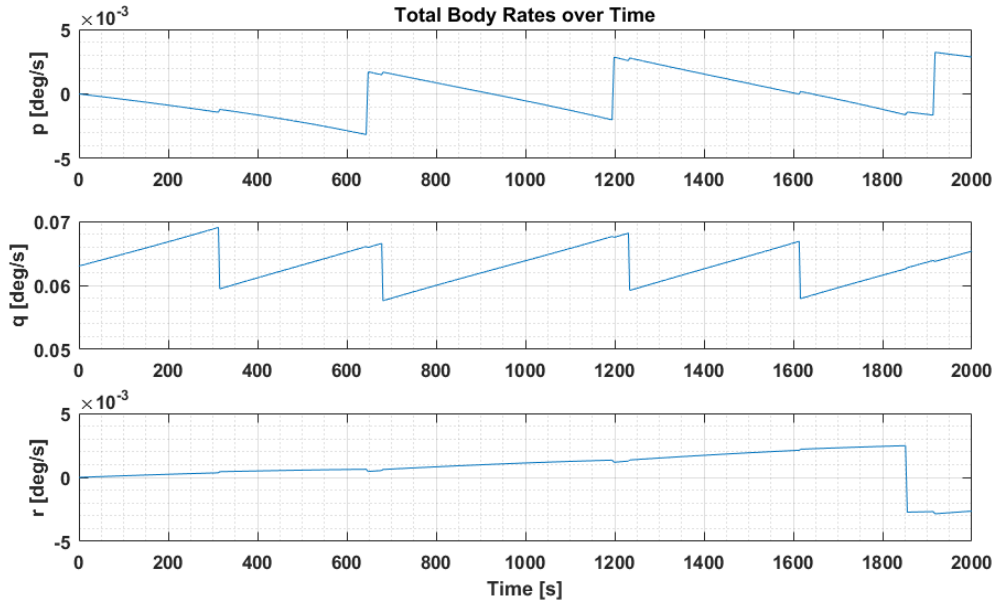

Figure 9. Body Rates with Respect to LVLH Frame with Phase Plane Control for Rigid-Body Motion

Figure 8 shows the results of the phase plane attitude hold controller on the attitude of the ISS body frame with respect to the LVLH frame. The phase plane controller successfully holds the spacecraft attitude along all axes to within 1 degree of the desired attitude, which is the expected result for a designed deadband of 1 degree. The body rate of the spacecraft as shown in Figure 9 displays spikes in rates corresponding with the controller torque outputs in Figure 10.

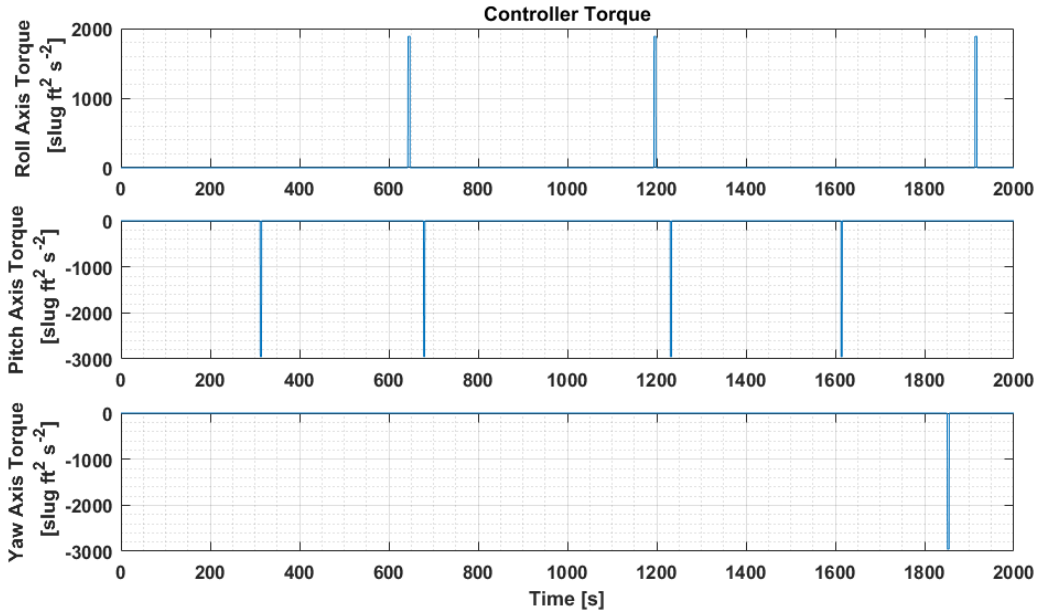

Figure 10. Control Torque Using Phase Plane Control for Rigid-Body Motion

Rigid and Flex

The developed flex filter is implemented on the CSIMSP with both rigid body and flex dynamics as well as gravity gradient torque. In this section, the results of implementing flex dynamics and the designed flex filter on both the PID controller and phase plane controller are shown and discussed. In all cases, the starting attitude and rate are $[\phi, \theta, \psi] = [5 \quad -5 \quad 5]$ deg. and $\boldsymbol{\omega} = [0 \quad 0.063 \quad 0]$ deg/s. The CSIMSP models a maneuver and attitude hold to $[\phi, \theta, \psi] = [15 \quad 15 \quad -15]$ deg.

In implementing both controllers, a zero-order hold is applied to represent the effect of a set sampling time. The PID controller is given a hold time, dt, of 1 second and the phase plane controller is given $dt = 0.2$ seconds. This is a means to make the controllers comparable. The phase plane controller implemented in the CSIMSP is full-on such that the maximum value of the output torques are always used during control, while the PID controller outputs a varying torque. By allowing the phase plane controller to "fire" more frequently, a more continuous signal is very roughly quantized.

PID Controller. Three different cases are investigated using the PID controller: 1) rigid-body only dynamics with no filter, 2) rigid and flex body dynamics with no filter, and 3) rigid and flex body dynamics with the designed flex filter.

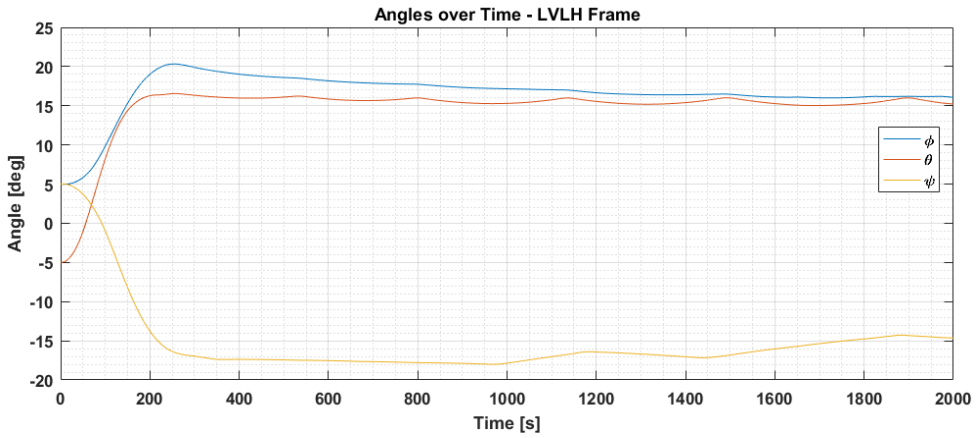

Figure 11. Body Rates with Respect to LVLH Frame with PID Control for Rigid-Body Motion

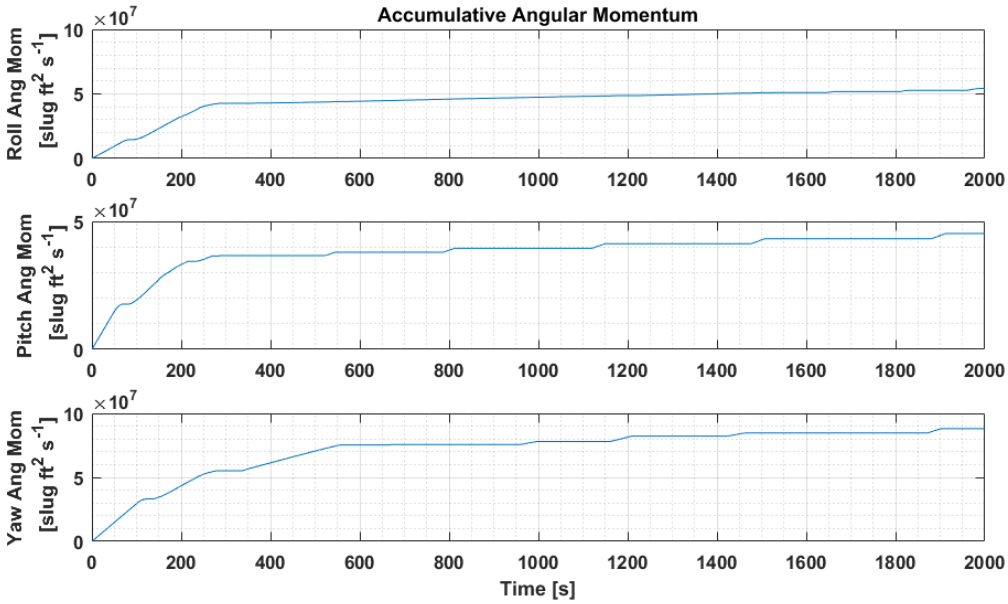

Figure 12. Accumulative Angular Momentum for PID Control for Rigid-Body Motion

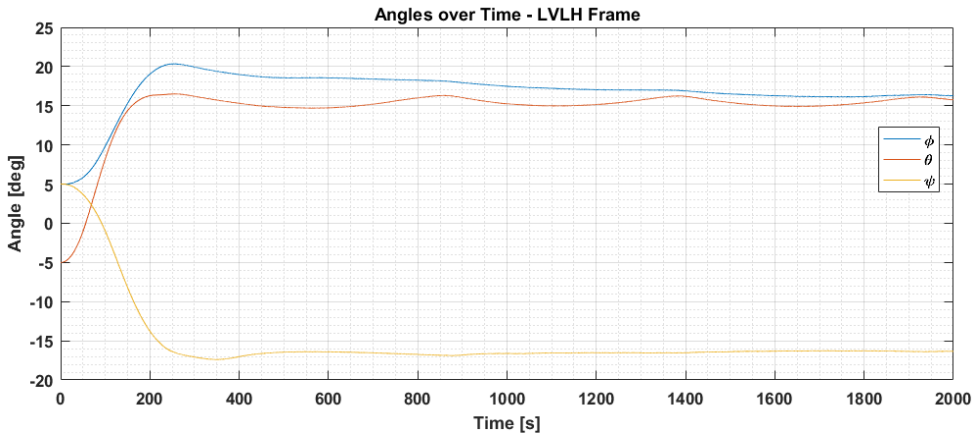

Figure 13. Body Rates with Respect to LVLH Frame with PID Control for Rigid and Flex Body Motion with No Filter

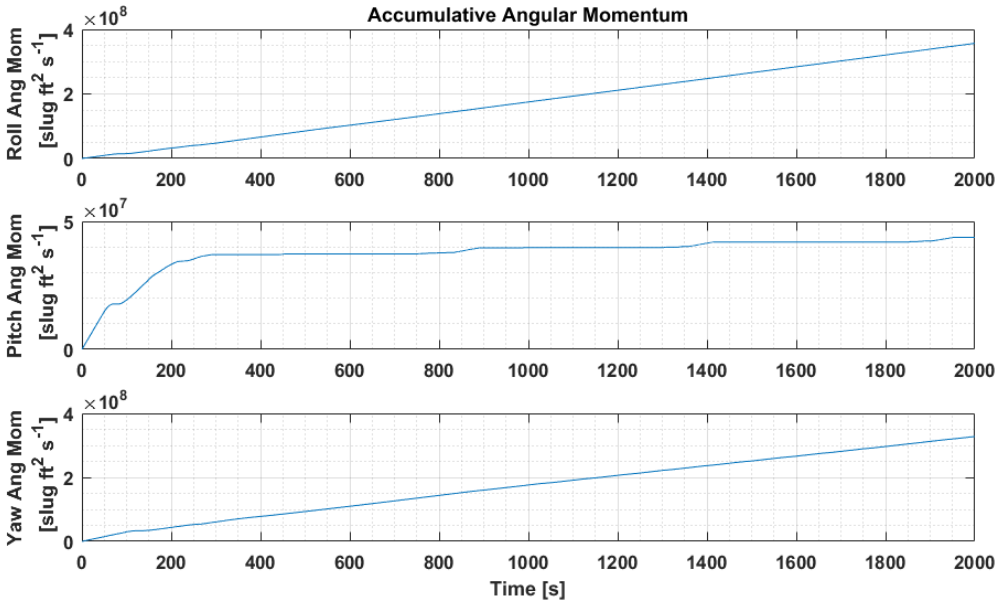

Figure 14. Accumulative Angular Momentum for PID Control for Rigid and Flex Body Motion with No Filter

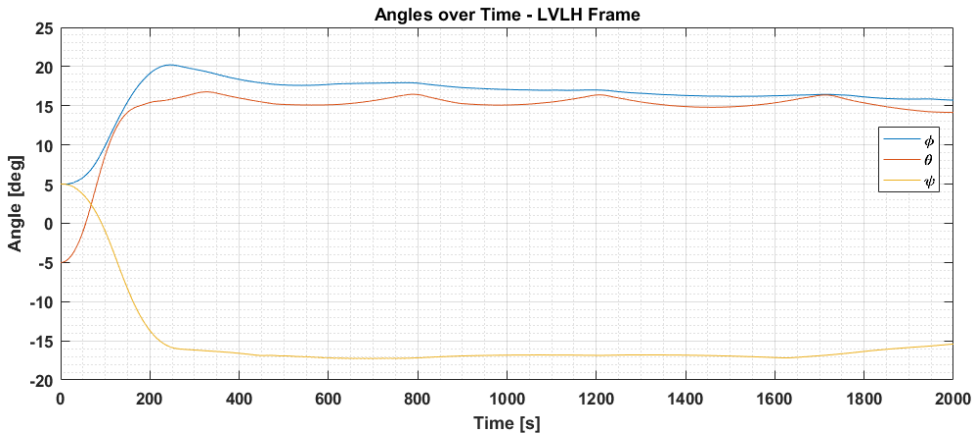

Figure 15. Body Rates with Respect to LVLH Frame with PID Control for Rigid and Flex Body Motion with Flex Filter

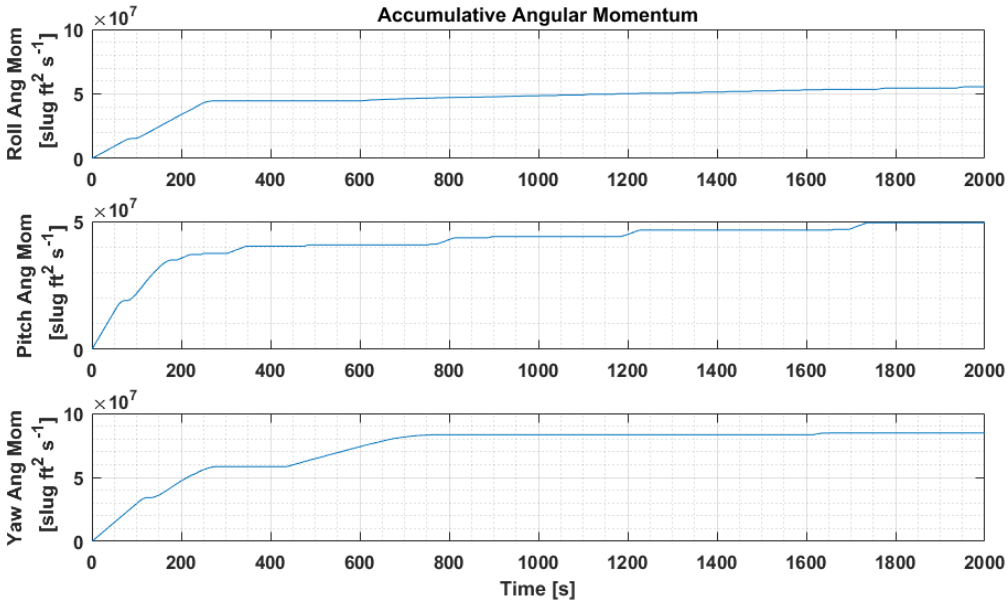

Figure 16. Accumulative Angular Momentum for PID Control for Rigid and Flex Body Motion with Flex Filter

In the case of the PID controller, the addition of the flex model and flex filter produces little effect in the controller's ability to maneuver the spacecraft or hold the attitude. Figure 12, Figure 14, and Figure 16 also show little difference in the accumulative angular momentum about the pitch axis between the cases. Including the flex dynamics model without flex filtering causes the accumulative angular momentum in the roll and yaw axes to grow steadily over time. This is indicative of a continuous firing about those axes to combat the flex dynamics contributions.

The effect of the flex filter becomes even more apparent when the load transformation matrix (LTM) outputs are studied. LTM outputs are produced by the flex dynamics model and give insight into the structural loads present on the modeled spacecraft. There are 19 groups of outputs, and all

output loads are normalized. A normalized load limit of 1 or greater indicates the load has exceeded the designed limit.

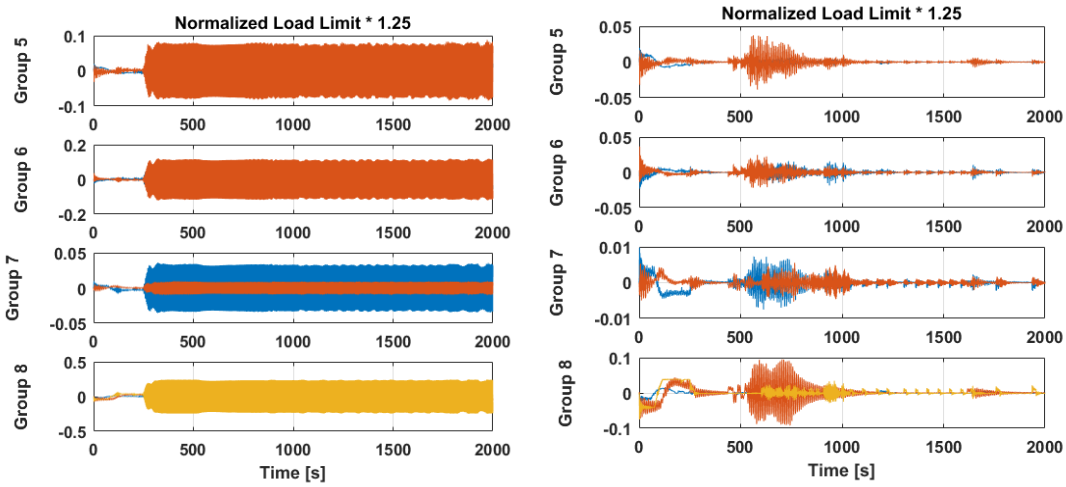

Figure 17. Groups 5-8 Load Response without (left) and with (right) Flex Filtering on PID Control

Figure 17 shows a comparison between the LTM outputs of groups 5-8 with and without flex filtering. It is clear that the addition of filtering prevents the load from growing over time by reducing and effectively eliminating high-frequency flex dynamics effects on the load outputs.

Phase Plane Controller. Two different cases are investigated using the phase plane controller: 1) rigid-body-only dynamics with no filter, and 2) rigid and flex body dynamics with the designed flex filter.

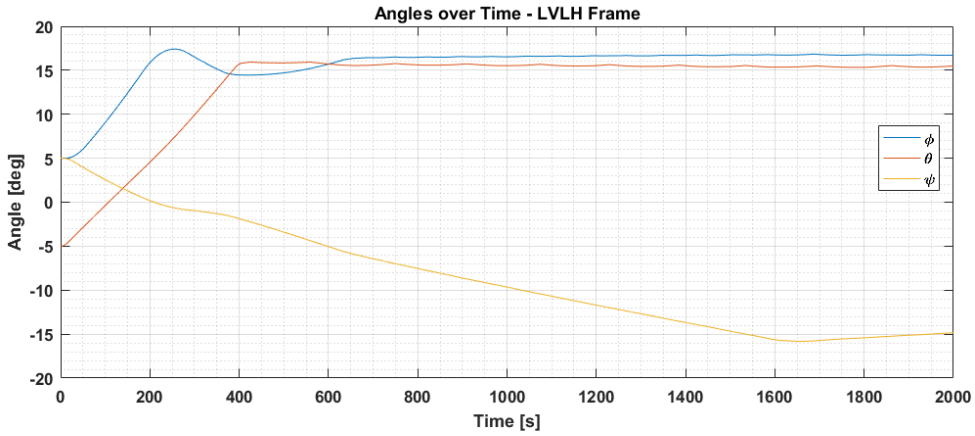

Figure 18. Body Rates with Respect to LVLH Frame in Phase Plane Control for Rigid-Body Motion

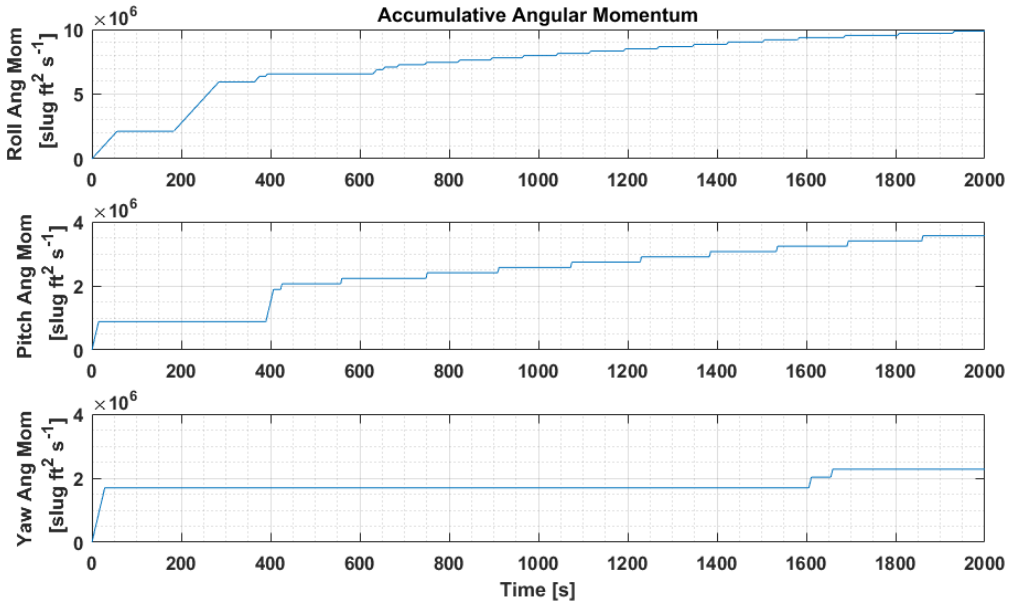

Figure 19. Accumulative Angular Momentum for Phase Plane Control for Rigid-Body Motion

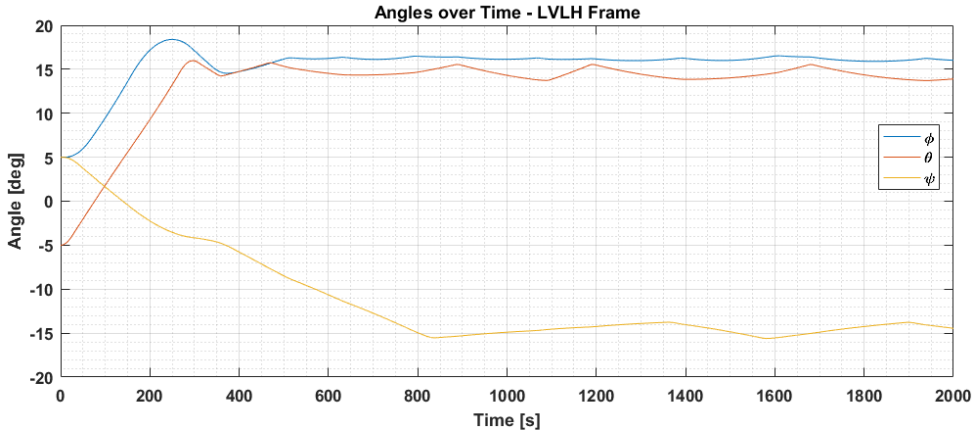

Figure 20. Body Rates with Respect to LVLH Frame with Phase Plane Control for Rigid and Flex Body Motion with Flex Filter

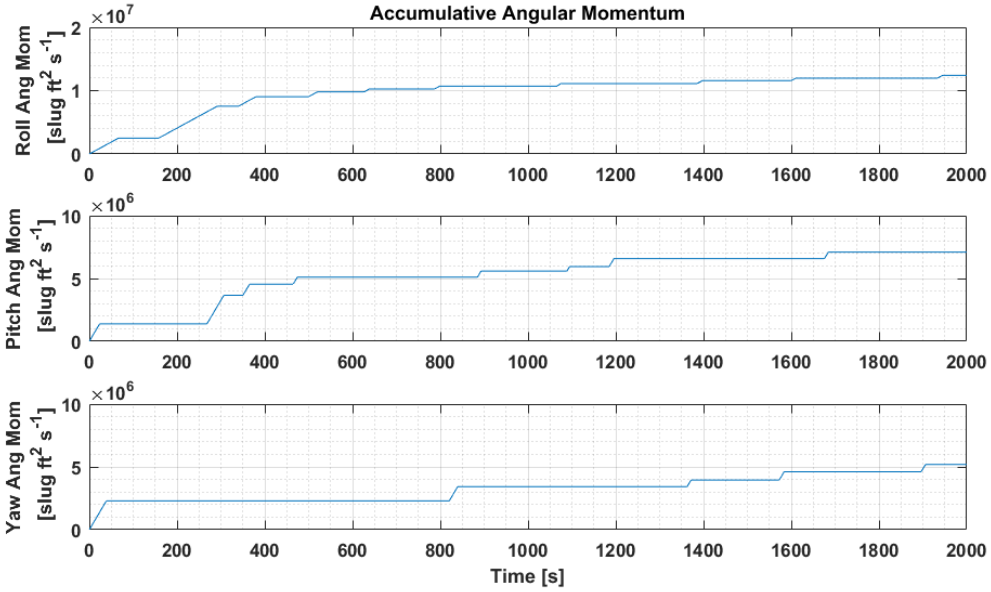

Figure 21. Accumulative Angular Momentum for Phase Plane Control for Rigid and Flex Body Motion with Flex Filter

A comparison of Figure 18 and Figure 20 shows that pitch, roll, and yaw control performance is better in the case of rigid-only dynamics, which is expected. The figures also show that the yaw angle is controlled to the desired attitude much faster in the case of flex dynamics and flex filtering. A comparison of Figure 19 and Figure 21 also shows that the case of rigid-only dynamics also produces less accumulative momentum in all channels than the case of flex dynamics with filtering. This is especially obvious in the pitch channel angular momentum.

PID and Phase Plane Control Comparison. The results of the previous section show there is a clear difference in the maneuver and attitude hold performance of the PID controller and phase plane controller. Two additional performance measures are used for direct comparison between the two controllers: accumulated angular momentum and load transformation matrix outputs.

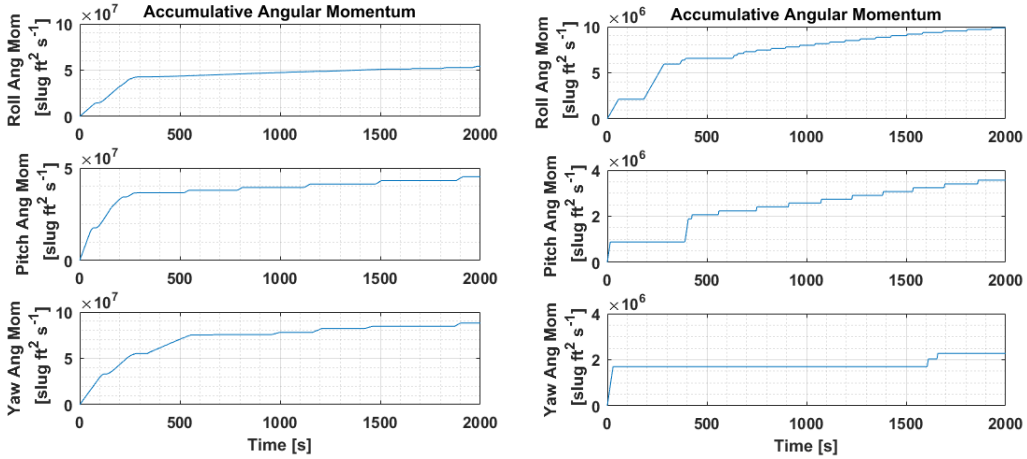

Figure 22. Accumulative Angular Momentum for PID (left) and Phase Plane (right) Control for Rigid-Body Motion

Figure 22 displays the accumulative angular momentum in the rigid-body dynamics only case for the PID controller and phase plane controller. In all three channels, the accumulated angular momentum is an order of magnitude smaller when implementing a phase plane controller. This also holds true for the case of implementing flex dynamics with a flex filter, shown in Figure 23.

The reduction in accumulated angular momentum is directly due to the difference in controller outputs. The PID controller outputs a continuous control torque in all three channels, producing a large continuous accumulated angular momentum. The phase plane controller outputs discontinuous control torques that appear as step functions with a minimum duration of the 0.2 second sample time. This design models thruster firing more realistically than the PID control continuous torque output.

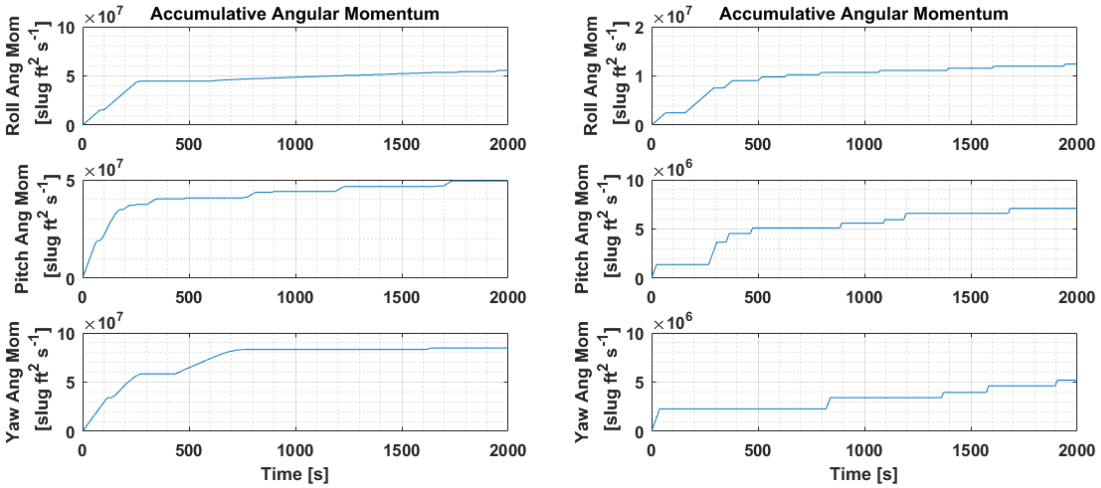

Figure 23. Accumulative Angular Momentum for PID (left) and Phase Plane (right) Control for Rigid and Flex Body Motion with Flex Filter

The LTM outputs for similar cases can also be compared. LTM outputs are produced by the flex dynamics model and give insight into the structural loads present on the modeled spacecraft. There are 19 groups of outputs, and all output loads are normalized. A normalized load limit of 1 or greater indicates the load has exceeded the designed limit.

Figures 24-28 present a comparison of the normalized load limits when PID control is applied and when phase plane control is applied. In each load group, the performance of the two controllers is relatively similar; the normalized loads in each group are of the same order of magnitude between controllers and are nearly all bounded by the same values between controllers. For the case of PID control, the controller appears to attenuate all structural loads to near zero by the end of the simulation time. There are small spikes periodically in the load responses in all groups, with the loads growing largest at the same time marker in the simulation. In the case of phase plane control, there are also periodic spikes in the load response of a larger magnitude than the spikes in the PID controller case. However, neither controller manages to attenuate the response consistently better than the other.

In both cases, the periodic spikes in the normalized loads response are likely due to the deadbands implemented in each controller. Any control torque output by either controller is sufficiently "large" enough to excite the flex dynamics frequency enough to be seen in the loads responses.

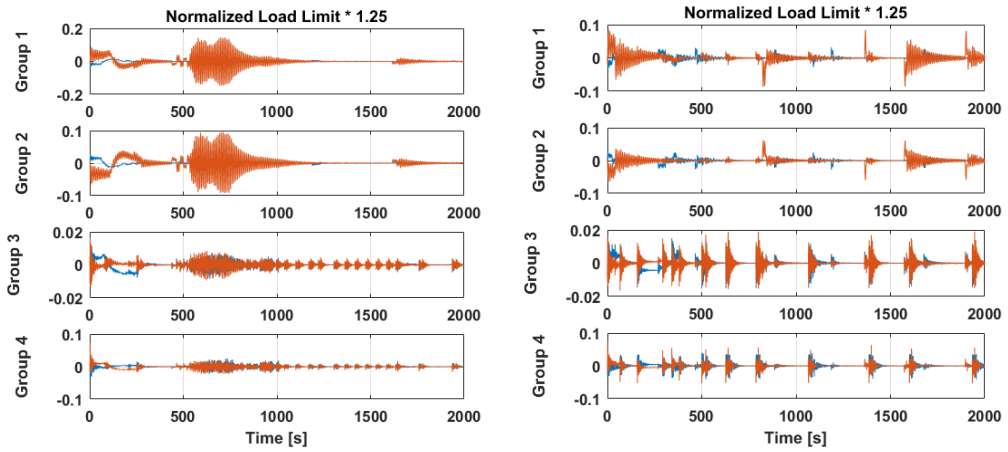

Figure 24. Groups 1-4 Normalized Loads Response for PID (left) and Phase Plane (right) Control for Rigid and Flex Body Motion with Flex Filter

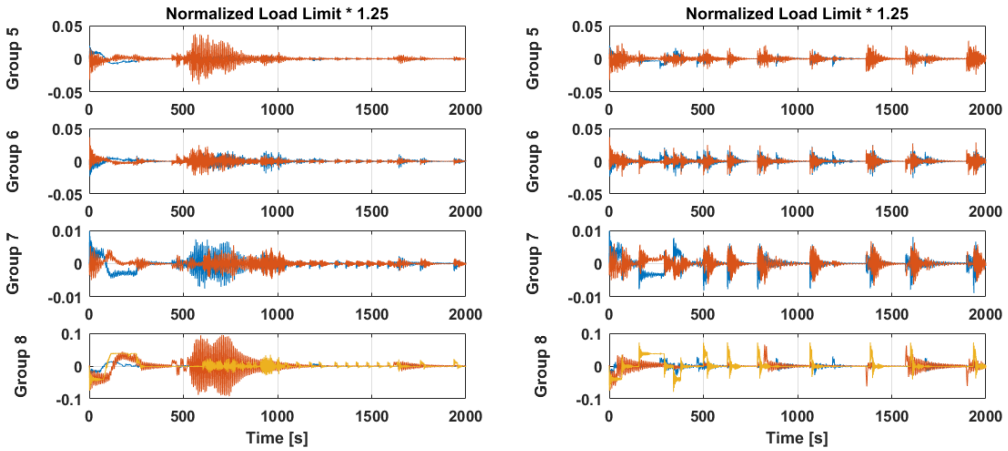

Figure 25. Groups 5-8 Normalized Loads Response for PID (left) and Phase Plane (right) Control for Rigid and Flex Body Motion with Flex Filter

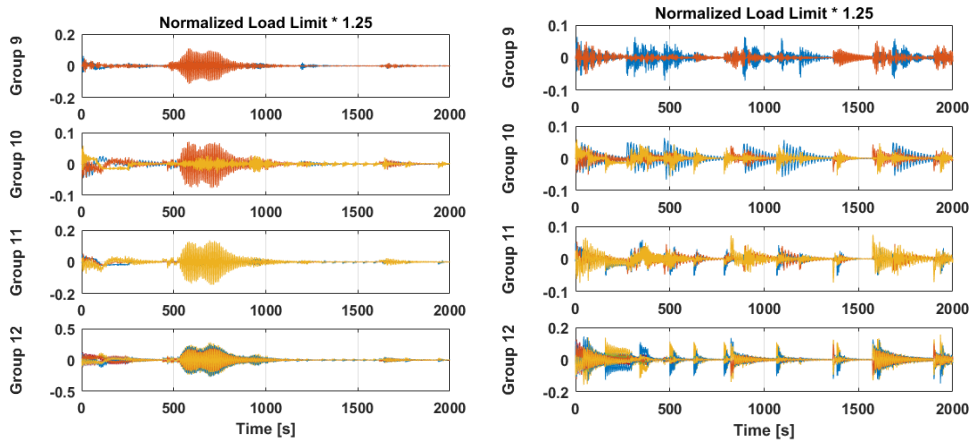

Figure 26. Groups 9-12 Normalized Loads Response for PID (left) and Phase Plane (right) Control for Rigid and Flex Body Motion with Flex Filter

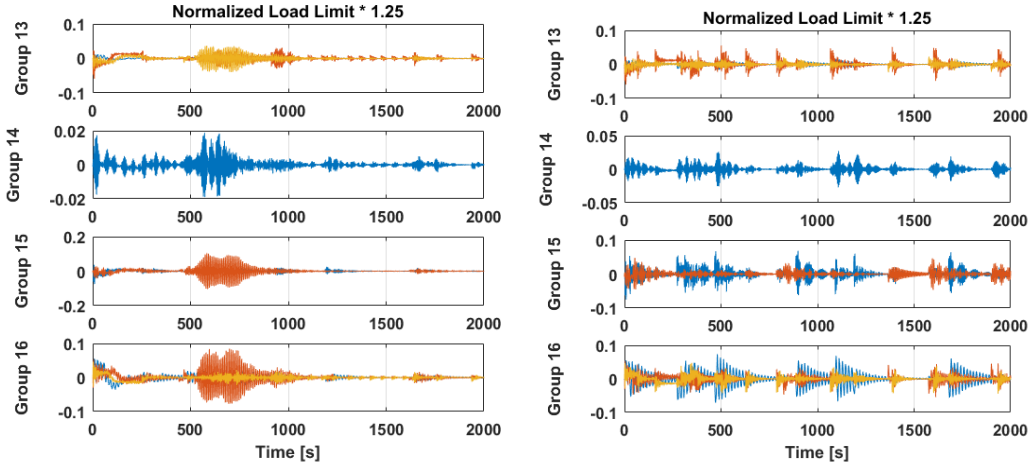

Figure 27. Groups 13-18 Normalized Loads Response for PID (left) and Phase Plane (right) Control for Rigid and Flex Body Motion with Flex Filter

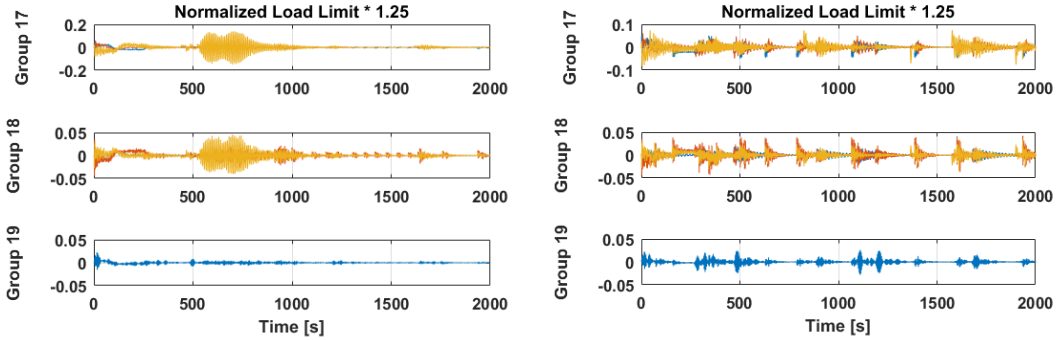

Figure 28. Groups 17-19 Normalized Loads Response for PID (left) and Phase Plane (right) Control for Rigid and Flex Body Motion with Flex Filter

The results herein are specific to the one case examined, and comparing the PID controller and phase plane controller results for a different attitude maneuver may yield a different conclusion about their performance relative to one another. Future work should also include a comparison of several different maneuver cases to produce a more robust comparison of the presented methods.

CONCLUSION

This work develops a testing platform for and trade study of control-structure interaction (CSI) mitigation techniques for flexible spacecraft such as the ISS. The platform developed in this work demonstrates the effectiveness of each chosen CSI mitigation strategy. For rigid-body motion, the designed PID controller effectively controls the ISS attitude to the desired attitude. The designed phase plane controller also produces similar results. In addition, the flex filter effectively reduces the effect of high-frequency flex dynamics on control of the system.

A comparison of the CSI mitigation strategies developed in this work shows both the PID and phase plane controllers are comparably effective in controlling spacecraft attitude and reducing structural loads produced by spacecraft flex dynamics. The phase plane controller is shown to produce significantly less accumulated angular momentum, which translates to less propellant usage by the control system. Future work should consist of adding variable output torque logic to the current full-on phase plane controller and comparing the PID and phase plane controller results for many different maneuver cases.

The studied CSI mitigation techniques have immediate applicability to the development of ISS on-orbit augmented control systems utilizing current and in-development visiting vehicles. In the future, this trade study of CSI mitigation solutions can be utilized to guide the design of ISS de-orbit control as well as Lunar Gateway rendezvous, proximity operations, and docking (RPOD) systems. A deeper understanding of CSI mitigation solutions is beneficial during the design of augmented control systems, which allow for flexibility in the visiting vehicle configurations for any spacecraft.

REFERENCES

[1] J. Cheng, G. Ianculescu, C. Kenney, A. Laub, J. Ly, and P. Papadopoulos, "Control-Structure Interaction for Space Station Solar Dynamic Power Module," *Proceedings of the 30th IEEE Conference on Decision and Control*, Brighton, UK, Dec 1991.

[2] J. W. Jang, M. Plummer, N. Bedrossian, C. Hall, M. Jackson, and P. Spanos, "Absolute Stability Analysis of a Phase Plane Controlled Spacecraft," *Proceedings of the AAS/AIAA Space Flight Mechanics Meeting*, San Diego, California, USA, Feb 2010.

[3] N. S. Bedrosian, "International Space Station CMG Momentum Desaturation Design," *AIAA Guidance, Navigation, and Control Conference and Exhibit*, Denver, Colorado, USA, Aug 2000

[4] N. Bedrossian, J. W. Jang, A. Alaniz, M. Johnson, K. Sebelius, and Y. Mesfin, "International Space Station US GN&C Attitude Hold Controller Design for Orbiter Repair Maneuver," *2005 AIAA Guidance, Navigation, and Control Conference and Exhibit*, San Francisco, California, USA, Aug 2005.

[5] P. C. Hughes, *Spacecraft Attitude Dynamics*. Mineola, New York: Dover Publications, Inc., 1st ed., 2004.

[6] F. L. Markley and J. L. Crassidis, *Fundamentals of Spacecraft Attitude Determination and Control*. New York, New York: Springer, 1st ed., 2014.

[7] R. A. Hall, S. Hough, C. Orphee, and K. Clements, "Design and Stability of an On-Orbit Attitude Control System Using Reaction Control Thrusters," *AIAA Guidance, Navigation, and Control Conference*, San Diego, California, USA, Jan 2016.

[8] A. N. Penchuk, P.D. Hattis, and E. T. Kubiak, "A Frequency Domain Stability Analysis of a Phase Plane Control System," *Journal of Guidance, Control, and Dynamics.* Vol. 8, No. 1, 1985, pp. 50–55.